Sources of Mesoscale Variability of Gravity Waves. Part I: Topographic Excitation

GREGORY D. NASTROM

Department of Earth Sciences, St. Cloud State University, St. Cloud, Minnesota

DAVID C. FRITTS

Geophysical Institute, University of Alaska, Fairbanks, Alaska

(Manuscript received 11 January 1991, in final form 1 May 1991)

ABSTRACT

Aircraft measurements of winds and temperatures collected during the GASP program are used to study the effects of topography as a source of mesoscale variability. Variances of fluctuations at the mesoscale over rough terrain are enhanced up to nearly two orders of magnitude compared to nonsource regions in some cases and are frequently enhanced by an order of magnitude. The implications of these episodic enhancements of variances for the vertical transports of energy and momentum are considered in the framework of gravity wave theory. The observed flight data are used to estimate the momentum flux $\overline{u'w'}$ on several flight segments. Results show that the flux is generally negative with mean value -0.26 m^2 s^{-2} and with magnitudes ranging up to -1.5 m^2 s^{-2}. Spectral analysis shows that the largest contributions to the net flux come from horizontal scales of $\sim 25 < \lambda_x < 60$ km. Finally, the observed momentum fluxes are used to infer the anisotropy factor of gravity waves over rough terrain, which is found to be about 0.45.

1. Introduction

Several recent studies have shown that the transports of energy and momentum by vertically propagating internal gravity waves have significant impacts on the circulation of the atmosphere (McFarlane 1987; Rind et al. 1988; Miller et al. 1989; Laursen and Eliasen 1989; Shao and Hantel 1989). Bannon and Yuhas (1990) discuss the schemes used to parameterize mountain wave drag in a general circulation model, although their theoretical results could be compared with only very limited observed values. Despite the recognized importance of gravity wave processes to problems of the general circulation, relatively little is known of their source mechanisms and their relative strengths and frequencies of occurrence. Detailed studies on a broad scale have been hindered by lack of suitable mesoscale data, and most studies have relied upon special observational campaigns employing aircraft (e.g., Lilly and Lester 1974; Kennedy and Shapiro 1980; Bacmeister et al. 1990) or surface measurements (e.g., Gedzelman 1983). The detailed wind measurements becoming available from radar wind profilers are suitable for the study of mesoscale processes such as gravity waves (e.g., Fritts et al. 1990; Nastrom et al. 1990), but they are confined to specific geographic areas and thus do not sample all possible atmospheric conditions.

Corresponding author address: Dr. David C. Fritts, Geophysical Institute, University of Alaska, Fairbanks, AK 99775.

In the face of these observational problems, the data collected aboard aircraft during the Global Atmospheric Sampling Program (GASP) are useful because they represent a relatively copious source of information on mesoscale variability under a wide variety of conditions and locations. The flights on which GASP data were collected were usually of relatively long duration and were during all seasons, thus permitting us to contrast the observed variability at airline cruise altitudes under differing conditions of latitude, season, underlying terrain, and background weather conditions. In earlier papers we have considered the changes in the mean variance over rough terrain compared with over plains or oceans (Nastrom et al. 1987; Jasperson et al. 1990, hereafter JNF). The results show that the mean variance at scales from about 4 to 80 km is significantly larger over mountains compared to over oceans or plains. These results complement those from the time domain. For example, Canavero and Einaudi (1987) have shown that there are significant differences in surface pressure spectra over plains and over rough terrain, and Nastrom and Gage (1990) found evidence in a study of wind profiler observations for a high-frequency (gravity wave) enhancement of the frequency spectrum of winds in the upper troposphere over rough terrain. All of these studies clearly show that the average variances are larger over mountains.

For some applications, however, information more detailed than simple means of observed variances is needed. As discussed in JNF, assuming the observed mesoscale variations are due to gravity waves implies

that the relative transports of momentum and energy are not uniform. Rather, they depend in a nonlinear manner on the velocity variances, as well as on the anisotropy (A) and the intermittency (I) of such motions. Intermittency is the fraction of time during which significant forcing exists, and anisotropy is the fraction of excess westward- over eastward-propagating wave energy relative to the total, that is, $A = (u'^2_W - u'^2_E)/(u'^2_W + u'^2_E)$. JNF expressed these relationships as:

$$c_{gz}E_{(\text{mountains/oceans})} \sim I(R/I)^2 \quad (1)$$

$$\overline{u'w'}_{(\text{mountains/oceans})} \sim AI(R/I)^{3/2}, \quad (2)$$

where R is the mean enhancement of the variance over source regions compared to over nonsource regions [note that the factor A in Eq. (6) of JNF was an error]. We will assume in this study that the variance enhancements are due to enhanced gravity wave activity.

The changes in the variance between mountains and plains or oceans are not constant; over the mountains the variance is not always enhanced and over the plains and oceans it is not always small. It is thus of interest to show the typical degree of enhancement of variance over the mountains and to examine the meteorological conditions that suppress enhancement. Variance enhancements due to meteorological factors such as fronts, jet streams, and convection are studied in a companion paper (Fritts and Nastrom 1992). A case study approach is used in both papers.

Increased variances of the velocity do not necessarily imply increased momentum flux. For monochromatic waves the momentum flux depends on the relative phase of horizontal and vertical velocity perturbations as well as on their magnitudes. While a few estimates of momentum fluxes and velocity variances have been obtained during studies of special events (e.g., Lilly and Kennedy 1973), they may not be representative of the more general circumstances encountered on the majority of GASP flights. Thus, a second goal of the present paper is to estimate the vertical momentum flux per unit mass, $\overline{u'w'}$, due to the observed motions in an effort to relate our variance estimates to the magnitude of the momentum flux. Finally, estimates of $\overline{u'w'}$ together with variables of the background flow can be used to estimate the anisotropy factor A.

The GASP data and our basic analysis procedure are described in section 2. Two case studies of flights over rough terrain are presented in section 3, one case when the variance was enhanced and one case when it was not. Our calculations of the momentum fluxes and related variables are presented in section 4, and summary remarks and conclusions are given in section 5.

2. Data recording and analysis

The GASP program was conducted by NASA to collect measurements at airline cruise altitudes using instruments placed aboard B747 aircraft in routine commercial service. Detailed descriptions of the instrumentation, route maps, and other facets of GASP are given in JNF and references therein. Briefly, the observational phase of GASP lasted from March 1975 through July 1979. Wind and temperature measurements, together with data on location, altitude, accelerometer readings, etc., were taken off the aircraft's inertial navigation system (INS). Winds were recorded to the nearest knot (about 0.5 m s^{-1}) and temperatures to the nearest degree celsius. Information on cloud particles and the concentrations of trace species such as ozone was obtained from special instruments placed aboard the aircraft.

All data were recorded on tape during flight above 6-km altitude and the tapes were later returned to NASA for data quality control and archiving. During archiving, tropopause pressures for each GASP data location were space and time interpolated from NMC grids and merged with the other GASP data. There are 6945 flights in the GASP dataset. During normal flight conditions data were recorded at 5-minute intervals (75 km at 250 m s^{-1} ground speed). However, data were recorded at 4-second intervals (1 km) on about 100 selected flights and on all flights during periods when moderate or greater turbulence was indicated by the vertical accelerometer reading. In this study we use only those flights with high-frequency data.

Mesoscale variances and spectra were computed over flight segments 64 and 256 km in length. Flight segments were not used for analysis if the aircraft pressure altitude changed by over 100 m or if a data gap greater than 4 (10) km was encountered. Along each segment retained for analysis, linear trends were removed from the zonal and meridional wind speeds and potential temperatures and the residuals were linearly interpolated to a 1-km grid for analysis with an FFT routine. 3411 (382) 64-km (256-km) segments were analyzed. Other details follow JNF.

3. Case studies of the effects of terrain on mesoscale variability

Two cases will be presented. The first case illustrates the very strong link between the magnitude of the variance and the presence of rough terrain, and is fairly typical of conditions usually encountered on GASP flights. The second case study includes a portion of a flight over rough terrain when the GASP variances remained relatively small. It illustrates the meteorological conditions that suppress a strong response at airline cruise altitudes to rough terrain below.

a. Variance enhanced by rough terrain

This case uses a flight from Honolulu to Chicago on 5 December 1978. Data suitable for this study were recorded from slightly west of Monterey, California,

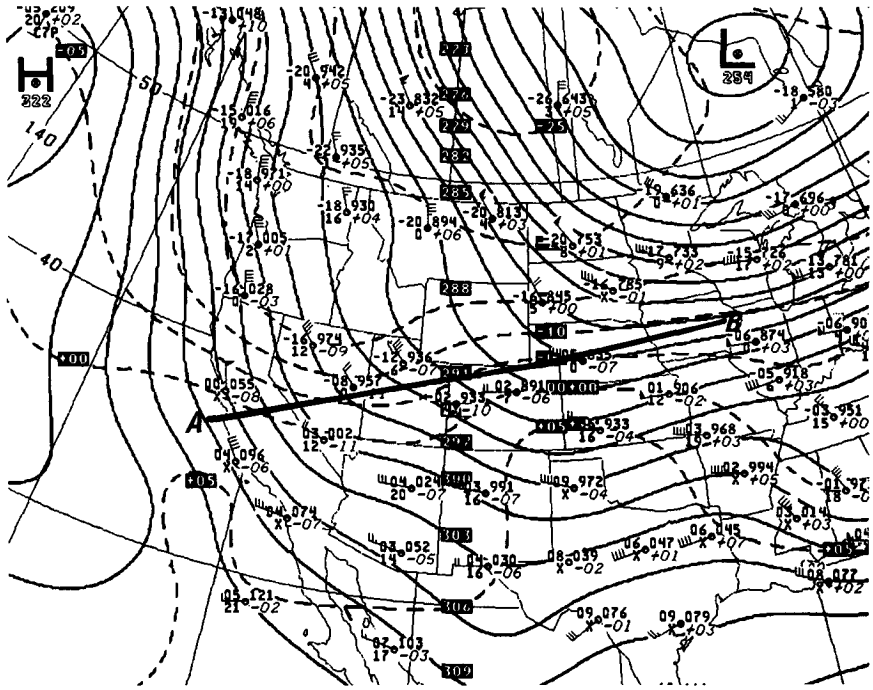

FIG. 1. 700-mb heights (dm) and temperatures (°C) at 1200 UTC 5 December 1978. Data suitable for this study were recorded along line AB on a GASP flight from Honolulu to Chicago.

to near Cedar Rapids, Iowa (from 36.52°N, 123.41°W to 42.11°N, 92.75°W), as shown by the aircraft track plotted in Fig. 1. The flight was undercast with clouds, with scattered showers reported at the surface along a quasi-stationary front stretching from California to Colorado and along a weak warm front from Colorado to Iowa. The flow at 700 mb, near 3-km pressure altitude (Fig. 1), was dominated by a deep trough over North America with a low centered near James Bay. Around the trough, winds were from the northwest over the mountain states and became nearly eastward over Iowa. At 200 mb, near 11.7-km pressure altitude (not shown), winds were nearly eastward from Nevada to Iowa. The maximum wind speeds at 200 mb were slightly north of the aircraft flight track, along the Nebraska–South Dakota border, about 60 m s^{-1}. The aircraft flight level pressure was 216 mb (pressure altitude 11.3 km).

The zonal wind speeds observed by the aircraft are shown in Fig. 2. Also shown are the mean terrain ele-

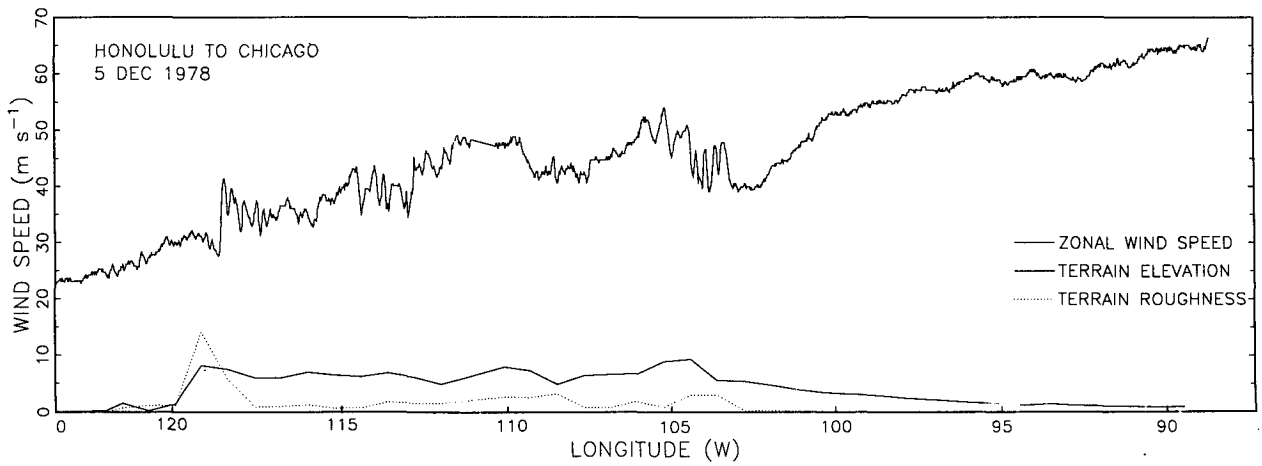

FIG. 2. Zonal wind speed at 11.3 km measured by the aircraft along the flight track shown in Fig. 1. Terrain elevation and the terrain roughness parameter are given in relative units (see text).

vation and the terrain roughness parameter at 64-km intervals. The terrain data are from the U.S. Navy 10 Minute Elevation Dataset described in JNF. The roughness parameter is the small-scale parameter, defined in JNF, which is related to the average terrain variance of 10′ × 10′ cells within each 1° × 1° area. The wind speed observations are spaced at approximately 1.2-km intervals, except near 111°W where there is a gap of about 50 km due to missing observations.

Inspection of Fig. 2 reveals relatively small velocity fluctuations west of about 119°W and east of about 105°W, and enhanced fluctuations over the mountainous terrain indicated by high elevation and increased values of the roughness parameter. The sudden changes in wave activity at the edges of the mountain regions are shown in greater detail in Fig. 3. The mean terrain height appears stepwise because it is available only each 10′ (about each 14 km at these latitudes), although the spacing of changes is shorter when the aircraft track crosses the corners of grid squares. The increased wave activity first appears about 25 km east of the first ridge of mountains in Fig. 3a, and it ends about 25 km east of the last large decrease in terrain height in Fig. 3b. The variations of zonal wind speed are nearly sinusoidal at the edges of the mountains, with wavelengths of about 25 km, and show a rich spectrum of wavelengths at intermediate locations.

Variances of zonal and meridional wind speed and potential temperature for 64-km segments of this flight are plotted in Fig. 4. The sudden changes of variance at the edges of the mountains are apparent in all variables. Jasperson et al. found that the average variance over mountains was increased by a factor of 2.6 compared to the average variance over the oceans, and over the roughest terrain defined by the roughness parameter discussed above the enhancement factor was 3.4 in the troposphere and 2.9 in the stratosphere. For the data in Fig. 4, the mean variance over the mountains is 16.8 times greater than the mean variance over the plains east of 103°W, and on individual segments the variance of zonal wind speed reaches 9.5 $m^2 s^{-2}$, about 56 times greater than that over smooth terrain. These results are summarized in Table 1.

The results for this case are fairly typical, as shown by the summary of flights in Fig. 5. These data represent all flights that crossed 105°W between 36° and 42°N, and did not cross a front or a region of thunderstorms and convection over the plains east of 105°W. It is shown in the companion paper that meteorological features such as fronts and convection may also lead to enhanced variances at airline flight altitudes. The mean variance over the mountains of the flights in Fig. 5 is enhanced by a factor of 5.1 (2.6) for the zonal (meridional) wind relative to that over smooth terrain. Note, however, in Fig. 5 that the variances are often enhanced by more than a factor of ten over the mountains, compared to over the plains or the ocean region

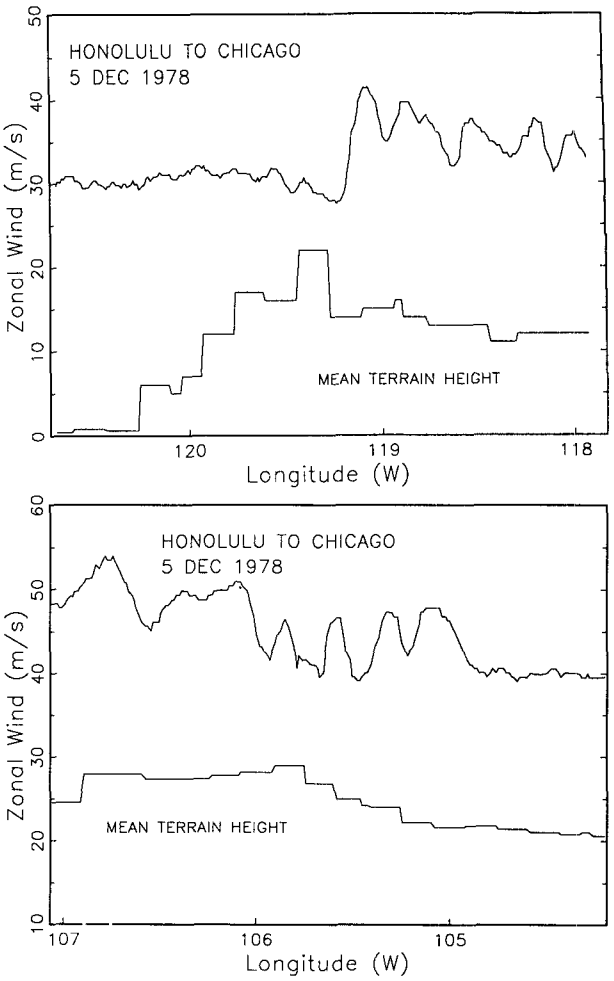

FIG. 3. Segments of the flight data shown in Fig. 2 at the edges of the mountains. Terrain height is in relative units.

west of the mountains. The peak enhancements relative to other regions are 42.9 and 14.6 for the zonal and meridional winds, respectively.

Even larger variances than those in Fig. 5 were encountered on some flight segments in parts of the world where the available meteorological data are not sufficient to identify clearly the source of the disturbance. The largest wind variance, 30.3 $m^2 s^{-2}$, is about two orders of magnitude larger than the mean variances over nonsource regions. The transport of momentum and energy during such episodes may be magnified nonlinearly, as discussed further below.

b. Meteorological conditions when variance is not enhanced

There are a few cases in Fig. 5 when the variances over the mountains are not enhanced, and it is of some interest to examine the meteorological conditions as-

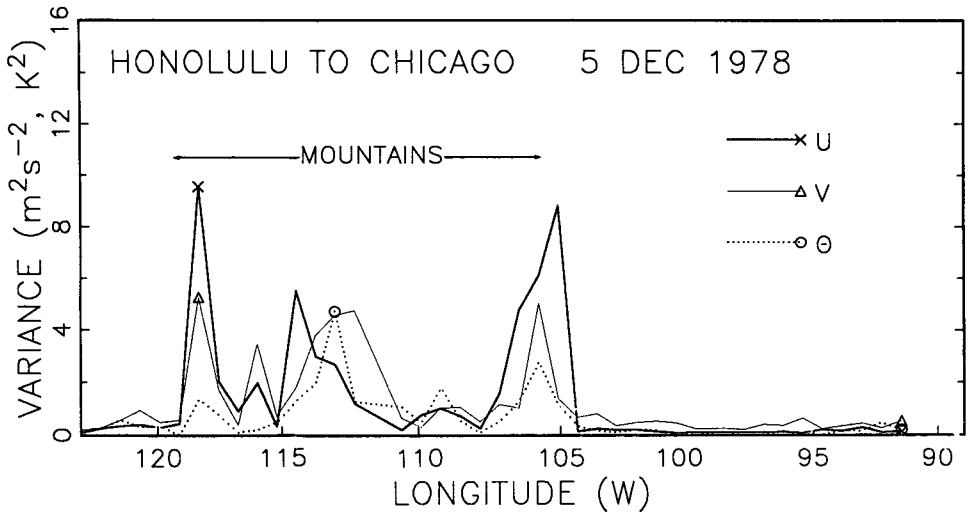

FIG. 4. Variances of zonal and meridional wind speed and of potential temperature over 64-km segments for the flight track shown in Figs. 1 and 2.

sociated with the differing responses. For example, Fig. 6 shows the variances of wind and temperature along a flight from New York to Los Angeles on 2 November 1978. The aircraft flight track is plotted in Fig. 7. The flight level pressure was 193 mb (11.9-km pressure altitude).

The variances seen in Fig. 6 west of about 110°W are typical of the mountain region seen in Fig. 5, but everywhere east of about 110°W they are relatively small even though the flight crossed the rugged Colorado Rockies very near Pikes Peak. The 700-mb chart at this time (Fig. 7a) shows relatively weak flow over Colorado with a weak short-wave ridge moving into this area. The ridging action is reflected by a small high pressure center at the surface, as seen in Fig. 7b. Apparently, light winds near local terrain height launch only weak disturbances, and the very stable air in the lower troposphere associated with the ridge system suppressed any convection near the surface. In fact, in each case where the variance over the very rough terrain near 105°W was not enhanced, there were relatively low wind speeds near the local terrain height at 700 mb and high static stability in the lower troposphere (below 500 mb).

While these results clearly point to the conditions when variances at airline cruise altitudes are not enhanced over rough terrain, it may not be appropriate to extrapolate them to general conditions. For example, from studies of profiler wind data, Ecklund et al. (1982) found that the variance of vertical velocity, an indicator of gravity wave activity, correlated closely with the 500-mb zonal wind speed at all times, apparently regardless of stability, and Nastrom et al. (1990) found that reduced gravity wave activity over the Flatland radar in Illinois was associated with high static stability at low altitudes, apparently regardless of wind.

TABLE 1. Average variance (m^2 s^{-2}) on 64-km flight segments over mountainous terrain compared with over oceans or plains. Results from Jasperson et al. (1990), JNF, are included for comparison. Values in parentheses are the mean variances over "rough" mountains (for JNF) or the largest variance observed in this study.

	Zonal wind			Meridional wind		
Data source	Average low variance	Average high variance	Ratio high/low	Average low variance	Average high variance	Ratio high/low
JNF (troposphere)	0.38	0.99 (1.30)	2.6 (3.4)	0.39	0.82 (1.09)	2.1 (2.8)
JNF (stratosphere)	0.48	1.31 (1.37)	2.7 (2.9)	0.56	1.16 (1.23)	2.1 (2.2)
HNL to ORD (see Fig. 3)	0.17	2.85 (9.56)	16.8 (56.2)	0.43	2.14 (5.27)	5.0 (12.3)
This study (see Fig. 5)	0.34	1.72 (14.6)	5.1 (42.9)	0.48	1.27 (7.02)	2.6 (14.6)

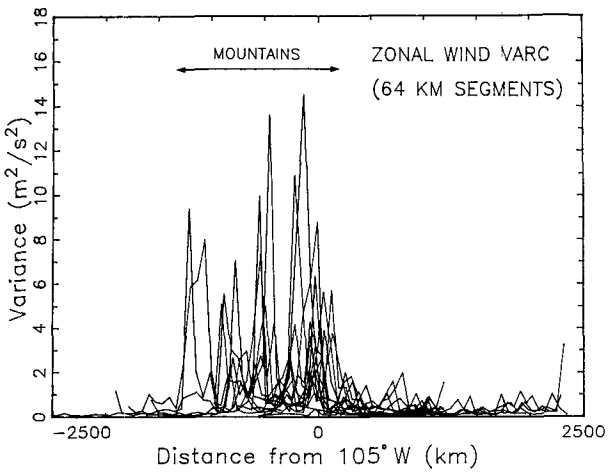

FIG. 5. Variance of zonal wind speed over 64-km segments for the 23 flights that crossed 105°W between 36° and 42°N and did not cross a front or convection over the plains. Values are plotted relative to 105°W.

4. Observations of the vertical flux of horizontal momentum

The mesoscale processes not resolved explicitly in numerical models of the atmosphere often require parameterization. Gravity waves are one such process, because of their strong influence on the atmospheric circulation at greater heights and their frequent occurrence at scales too small to be resolved in current large-scale circulation models. Thus, it would be useful if our observations of the magnitude of velocity variances could be related to the magnitude of the vertical flux of horizontal momentum. In order to relate our results to the implications of gravity wave theory, it will be necessary to assume the enhanced variances are due to gravity waves, following JNF.

Following Lilly and Lester (1974) we estimate the vertical momentum flux, $\overline{\rho u'w'}$, from observations of the horizontal wind and potential temperature. Assuming isentropic flow, the equation for the conservation of potential temperature θ provides a relationship which can be solved for the vertical velocity

$$w' = -(\bar{u} - c)\frac{\partial\bar{\theta}/\partial s}{\partial\bar{\theta}/\partial z}, \tag{3}$$

where $\bar{u}$ is the wind speed parallel to the mean flow, $\partial\bar{\theta}/\partial s$ is the gradient along the flow, and c is the phase speed of gravity waves. Here c is assumed to be zero for waves excited by topography.

Equation (3) was applied to GASP observations along 256-km segments; $\partial\bar{\theta}/\partial z$ was interpolated from balloon observations to the beginning of each segment. Assuming the flow is steady and two-dimensional, w' was derived using the continuity equation to define a streamfunction ψ such that $\rho\bar{u} = \partial\psi/\partial z$, $\rho w = -\partial\psi/\partial s$, and $\rho\bar{u}/(\partial\bar{\theta}/\partial z) = d\psi/d\bar{\theta}$, so that

$$w' = -(d\psi/d\bar{\theta})\frac{\partial\bar{\theta}}{\rho\partial s}. \tag{4}$$

The momentum flux per unit mass for each segment, $\overline{u'w'}$, was computed by averaging the product of the observed u' and the computed w' values at each point. For flights in the troposphere the variations of θ were usually so small that meaningful changes in w' could not be inferred. This method also is most reliable if the aircraft heading is within ~20° of the mean wind direction so that $u \sim V\cos(\Delta\phi)$, where V is the total

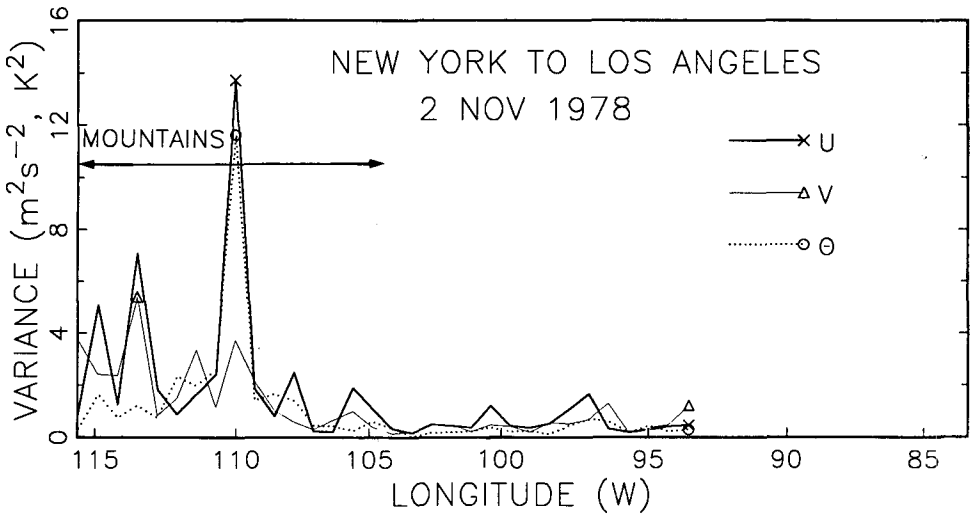

FIG. 6. As in Fig. 4, except for a flight from New York to Los Angeles on 2 November 1978 along the flight track given in Fig. 7. Note the variances are not enhanced over the mountains in the region of light winds and high static stability between 105° and 110°W.

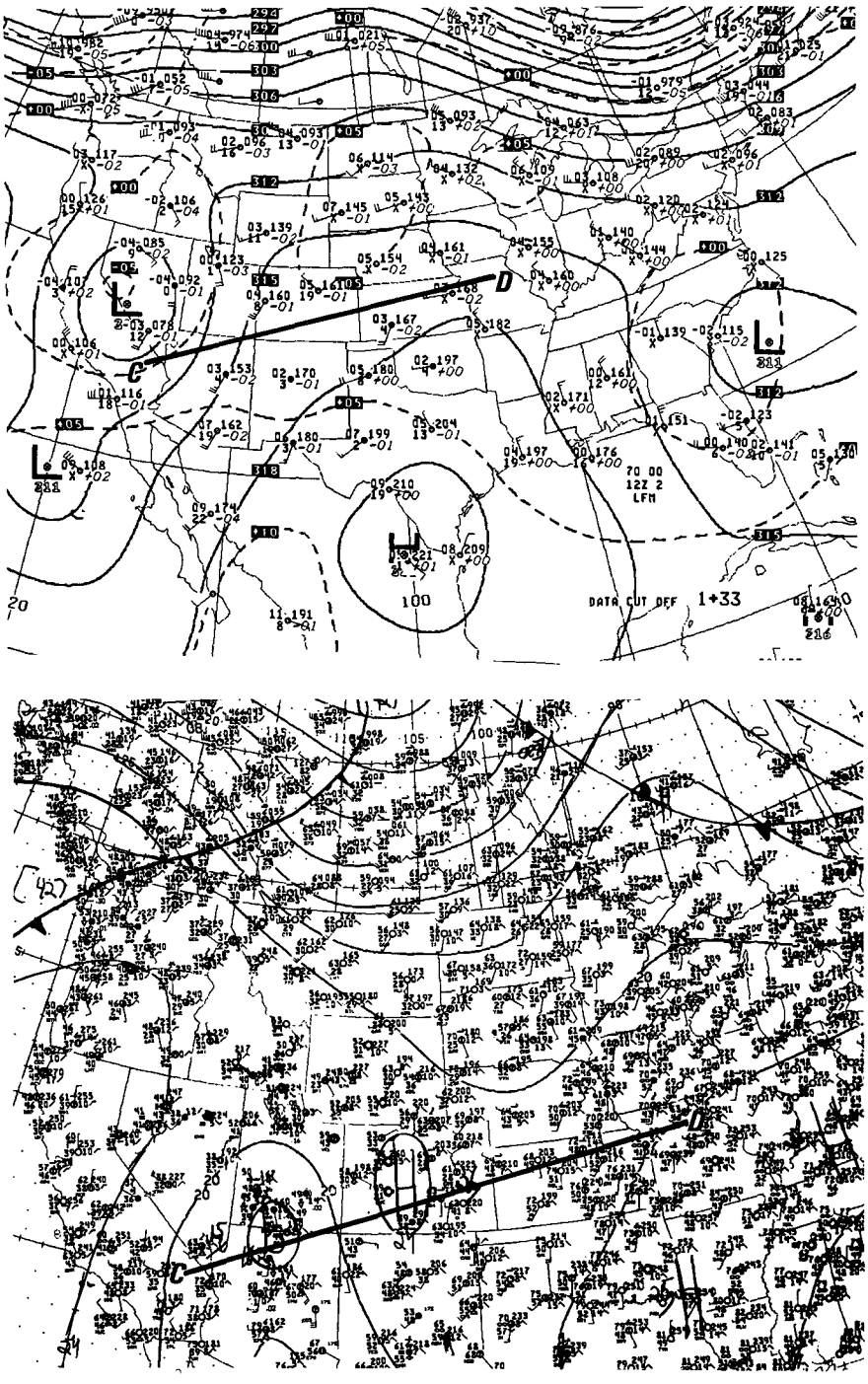

speed and $\Delta\phi$ is the angle difference. As a result of these constraints, and the requirement that flow systems not be changing rapidly so that the 12-hour balloon data could be interpolated with confidence, only a relatively few flight segments of our total sample over the western United States were suitable for computing momentum fluxes.

The momentum flux estimates are summarized in Table 2. Based on the coarse resolution of the temperature data, the uncertainty of these flux estimates

TABLE 2. Computations of momentum flux over the western United States on selected 256-km GASP flight segments.

Latitude (°N)	Longitude (°W)	σ_u^2 ($m^2 s^{-2}$)	σ_w^2 ($m^2 s^{-2}$)	$\overline{u'w'}$ ($m^2 s^{-2}$)	Flux ($N m^{-2}$)
37.8	119.3	6.7	0.8	−0.23	−0.078
38.2	117.9	5.5	1.9	−0.46	−0.152
38.5	116.5	3.2	1.0	−0.24	−0.080
40.0	110.1	2.9	3.0	0.08	0.027
40.5	107.2	8.0	2.3	−0.26	−0.088
40.6	106.3	13.2	3.6	−0.70	−0.229
40.9	104.1	7.3	1.9	−0.05	−0.016
37.5	122.8	1.5	0.2	−0.04	−0.013
38.4	120.1	7.3	0.7	−0.25	−0.086
39.2	117.2	5.8	3.4	−0.39	−0.138
39.9	114.3	3.7	0.1	−0.04	−0.014
40.5	111.4	10.9	0.2	−0.08	−0.029
41.4	105.5	8.6	0.5	−0.61	−0.196
39.8	112.7	3.6	0.2	−0.08	−0.027
35.4	118.5	0.3	0.2	−0.03	−0.011
36.3	115.8	0.6	0.1	0.01	0.004
38.0	110.2	3.8	0.5	−0.11	−0.040
38.7	107.3	9.3	1.4	−1.42	−0.490
39.3	104.4	5.0	0.5	−0.13	−0.045

is at least a factor of two, and may be greater if the assumptions of isentropic flow and zero phase velocity are violated. Nevertheless, the numerical values seem reasonable. Most values are negative, indicating an upward flux of westward momentum, consistent with past studies (e.g., Lilly and Kennedy 1973; Kennedy and Shapiro 1979). The largest magnitudes, found near 105°W and 117°W, are about −0.5 to −1.5 $m^2 s^{-2}$ (about −0.2 to −0.5 N m^{-2}), slightly less than the results of Lilly and Lester (1974), which were obtained at higher altitudes (about 14 to 18 km) in a very disturbed flow situation and ranged from about −0.1 to −0.3 N m^{-2}. If these represent limiting values both at 11.3 and 14 km, such a vertical divergence of momentum flux implies a body force per unit mass of about 20 m s^{-1} h^{-1}.

The spectra and cospectra of u' and w' for the four segments with the largest flux values are given in Fig. 8. The w' spectra appear to fall to a white noise value at wavenumbers $k > \sim 10^{-4}$ m^{-1} ($\lambda_x = 2\pi/k \sim 6$ km), suggesting a lower limit for the useful data. Cospectra are presented in both standard and in area-preserving form. The latter indicate that the flux is negative for $k < \sim 4 \times 10^{-4}$ m^{-1} ($\lambda_x \sim 15$ km), with the primary contributions to the integrated covariance occurring for $\lambda_x \sim 25$–60 km. This range of wavelengths likely represents a convolution between the spectral content of the underlying topography, which is increasing to at least 100-km wavelength (e.g., Bannon and Yulas 1990), and the general decrease of momentum flux with increasing wavelength due to the decreasing amplitude of the vertical velocity perturbations with wavelength.

The momentum flux values in Table 2 can be used to estimate the anisotropy of the gravity wave field, assuming the motions are due to gravity waves. Details of the linear gravity wave theory are reviewed by Fritts (1984). For a single wave propagating in the x–z plane with horizontal and vertical wavenumbers k and m and with phase speed ~ 0, the momentum flux is

$$\overline{u'w'} \sim \frac{u'w'}{2} \sim \frac{u'(-u'k)}{2m} \sim -u'^2 \frac{\bar{u}k}{2N}, \qquad (5)$$

where N is the Brunt–Väisälä frequency. If multiple waves are present and the energy is divided between waves propagating eastward and westward, then the anisotropy (A) of the wave field reduces the net momentum flux as

$$\overline{u'w'} \sim -Au'^2 \frac{\bar{u}k}{2N}, \qquad (6)$$

where $A \leq 1$; $A = 0$ corresponds to equally energetic eastward- and westward-propagating wave motions. In Fig. 3a over the Sierra Nevada $u \sim 35$ m s^{-1}, $u' \sim 2.5$ m s^{-1}, and $\lambda_x \sim 27$ km. The buoyancy period in the layer 200–250 mb is 425 s, giving

$$\overline{u'w'} \sim -1.7A.$$

The observed value in Table 2 is $(\overline{u'w'})_0 = -0.46$ $m^2 s^{-2}$, giving $A \sim 0.3$. Similarly, in Fig. 3b $\bar{u} \sim 45$ m s^{-1}, $u' \sim 2$ m s^{-1}, and $\lambda_x \sim 25$ km, giving

$$\overline{u'w'} \sim -1.5A.$$

Since in this case $(\overline{u'w'})_0 = -0.7$, we estimate $A \sim 0.5$.

Equation (6) implies that the momentum flux is related to the product $u'^2\bar{u}$, assuming the gravity wave theory is a valid model. The observed relationship between $\overline{u'w'}$ and $u'^2\bar{u}$ for all cases is shown in Fig. 9. The solid line fit to the edge of the cloud of available points apparently provides an estimate of the upper bound of A under general conditions. Assuming that the predominant $\lambda_x \sim 40$ km and $N \sim 0.02$ s^{-1} for stratospheric conditions, the line represents $A = 0.45$. This estimate is similar to those obtained above for individual cases. The lower boundary of the cloud of points in the corresponding plot of $\overline{u'w'}$ as a function of u'^2 (not shown) approximately follows a 3/2 power curve, consistent with the relationship expressed in Eq. (2). These comparisons show that the gravity wave model used here is consistent with our observations.

5. Summary and conclusions

Flight segments from GASP have been used to study the effects of topography as a source of mesoscale variability at airline cruise altitudes. In particular, case studies have been used to illustrate the wide range of conditions encountered and to highlight the effects of background meteorological conditions. In addition to

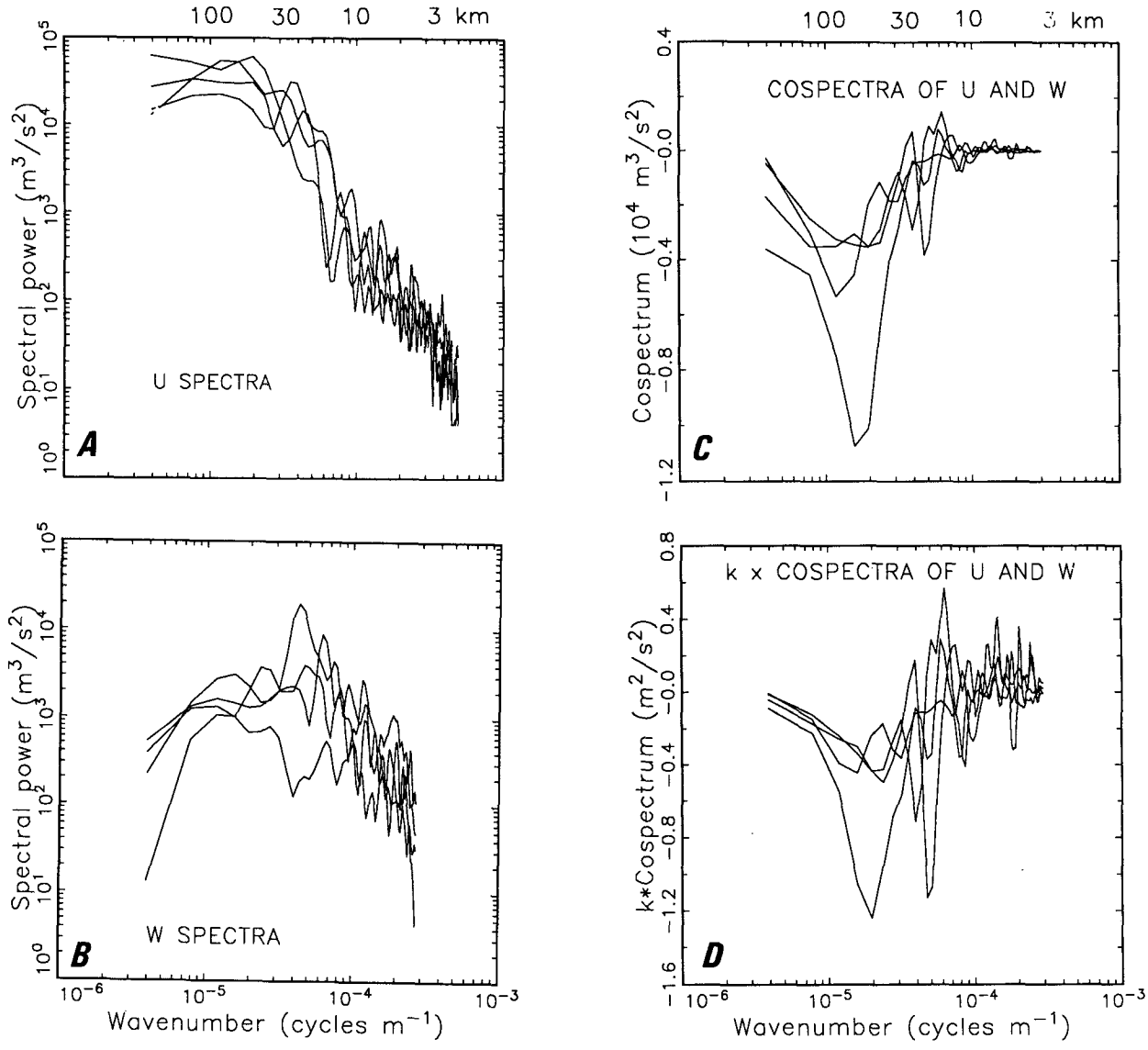

FIG. 8. Spectra and cospectra of wind speed along 256-km flight segments for four selected segments (a) u parallel to the flight track, (b) vertical velocity, (c) and (d) cospectra of u and w in standard and area-preserving coordinates, respectively.

the variances, we have estimated the momentum fluxes, $\overline{u'w'}$, on several flights. By relating the results to the linear theory of gravity waves we have estimated the anisotropy factor.

The following conclusions were reached:

1) The variance of zonal and meridional wind speeds and of potential temperature usually show marked increases over rough terrain. The magnitude of the variance can be over 50 times greater than the mean variance over flat terrain.

2) The variance over rough terrain is not enhanced relative to that over plains under synoptic conditions when there are relatively light horizontal winds at mountaintop heights and high static stability in the lower troposphere.

3) The vertical flux of zonal momentum is usually negative, with the largest values occurring near the edges of mountainous regions in our small sample of flights over the western United States. Observed values range from 0.01 to -1.42 m^2 s^{-2}, with mean value -0.26 m^2 s^{-2}.

4) Spectral analysis shows that largest contributions to the covariance of u' and w' come from wavelengths $25 < \lambda_x < 60$ km.

5) The magnitude of the vertical momentum flux on these flight segments has a maximum negative value related to the product $u'^2\bar{u}$. This relationship is con-

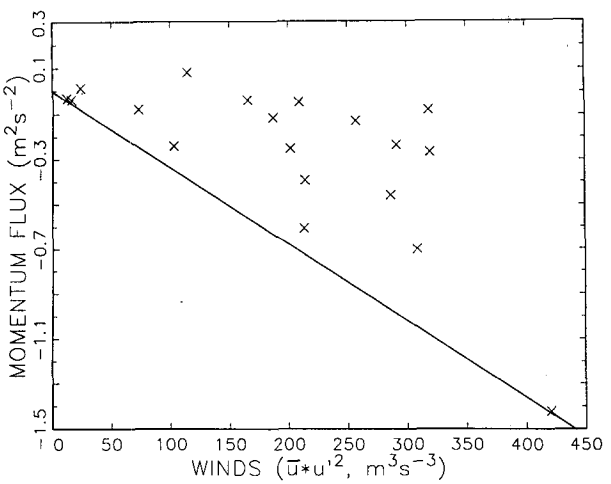

FIG. 9. Vertical momentum flux ($\overline{u'w'}$) as a function of the horizontal transport of variance ($u'^2\bar{u}$) for the 19 available flight segments over the western United States. The solid line is fit to the edge of the cloud of points and shows apparent bounding values of momentum flux.

sistent with the hypothesis that the motions are produced by gravity waves.

6) Assuming the momentum flux is due to upward-propagating gravity waves, the typical level of anisotropy is about 0.45.

Acknowledgments. Support for this work was provided by the National Aeronautics and Space Administration under Grant NAGW-1179.

REFERENCES

Bacmeister, J. T., M. R. Schoeberl, L. R. Lait, P. A. Newman, and B. Gary, 1990: Small-scale waves encountered during AASE. *Geophys. Res. Lett.*, **17,** 349–352.

Bannon, P. R., and J. A. Yuhas, 1990: On mountain wave drag over complex terrain. *Meteor. Atmos. Phys.*, **43,** 155–162.

Bedard, A. J., F. Canavero, and F. Einaudi, 1986: Atmospheric gravity waves and aircraft turbulence encounters. *J. Atmos. Sci.*, **43,** 2838–2844.

Canavero, F. G., and F. Einaudi, 1987: Time and space variability of spectral estimates of atmospheric pressure. *J. Atmos. Sci.*, **44,** 1589–1604.

Ecklund, W. L., K. S. Gage, B. B. Balsley, R. G. Strauch, and J. L. Green, 1982: Vertical wind variability observed by VHF radar in the lee of the Colorado Rockies. *Mon. Wea. Rev.*, **110,** 1451–1457.

Fritts, D. C., 1984: Gravity wave saturation in the middle atmosphere: A review of theory and observations. *Rev. Geophys. Space Phys.*, **22,** 275–308.

——, and G. D. Nastrom, 1992: Sources of mesoscale variability of gravity waves. II: Frontal, convective, and jet stream excitation. *J. Atmos. Sci.*, **49,**111–127.

——, T. Tsuda, T. E. VanZandt, S. A. Smith, T. Sato, S. Fukao, and S. Kato, 1990: Studies of velocity fluctuations in the lower atmosphere using the MU radar: Part II. Momentum fluxes and energy densities. *J. Atmos. Sci.*, **47,** 51–66.

Gedzelman, S. D., 1983: Short-period atmospheric gravity waves: A study of their statistical properties and source mechanisms. *Mon. Wea. Rev.*, **111,** 1293–1299.

Jasperson, W. H., G. D. Nastrom, and D. C. Fritts, 1990: Further study of terrain effects on the mesoscale spectrum of atmospheric motions. *J. Atmos. Sci.*, **47,** 979–987.

Kennedy, P. J., and M. A. Shapiro, 1980: Further encounters with clear air turbulence in research aircraft. *J. Atmos. Sci.*, **37,** 986–993.

Laursen, L., and E. Eliasen, 1989: On the effects of the damping mechanisms in an atmospheric general circulation model. *Tellus,* **41A,** 385–400.

Lilly, D. K., and P. J. Kennedy, 1973: Observations of a stationary mountain wave and its associated momentum flux and energy dissipation. *J. Atmos. Sci.*, **30,** 1135–1152.

——, and P. F. Lester, 1974: Waves and turbulence in the stratosphere. *J. Atmos. Sci.*, **31,** 800–812.

McFarlane, N. A., 1987: The effect of orographically excited gravity wave drag on the general circulation of the lower stratosphere and troposphere. *J. Atmos. Sci.*, **44,** 1775–1800.

Miller, M. J., T. N. Palmer, and R. Swinbank, 1989: Parameterization and influence of subgridscale orography in general circulation and numerical weather prediction models. *Meteor. Atmos. Phys.*, **40,** 84–109.

Nastrom, G. D., and K. S. Gage, 1990: Enhanced frequency spectra of winds at the mesoscale based on radar wind profiler observations. *Radio Sci.*, **25,** 1039–1048.

——, M. R. Peterson, J. L. Green, K. S. Gage, and T. E. VanZandt, 1990: Sources of gravity wave activity seen in the vertical velocities observed by the Flatland VHF radar. *J. Appl. Meteor.*, **29,** 783–792.

Rind, D., R. Suozzo, and N. K. Balachandran, 1988: The GISS global climate-middle atmosphere model. Part II: Model variability due to interactions between planetary waves, the mean circulation and gravity waves. *J. Atmos. Sci.*, **45,** 371–386.

Shao, Y., and M. Hantel, 1989: Vertical subsynoptic momentum flux in the atmosphere over central Europe. *Quart. J. Roy. Meteor. Soc.*, **115,** 1355–1372.